Supplementary Material to accompany the article "Effects of Cardiac Myosin Binding Protein-C on Actin Motility Are Explained With A Drag-Activation-Competition Model"

Sam Walcott, Steffen Docken and Samantha P. Harris

October 30, 2014

Overview

This supplement contains four main topics.

1. The first topic is a theory for the interaction of myosin with regulated thin filaments (actin with troponin and tropomyosin) in the presence of cMyBP-C (cardiac myosin binding protein-c). In sections 1–3, we derive and validate this theory.

2. The second topic is fitting the theory to experimental measurements of actin motility. In section 4, we describe pre-processing of the data, optimization of fit and a sensitivity analysis of model parameters. We were able to perform this analysis because our theory is efficient, lacks stochastic noise and can be non-dimensionalized to give a minimal parameter set. This analysis would be much more difficult, if not impossible, with Monte-Carlo simulations.

3. The third topic is fitting solution measurements of actin interacting with unregulated thin filaments (actin) in the presence of MyBP-C. In section 5, we describe our model, fit the model to data and present a sensitivity analysis.

4. The fourth and final topic is a description of our Monte-Carlo simulations in section 6. These were used primarily to validate the theory (in the previous sections), but we also use these simulations to prediction experimental results (in this section).

1 Theory I: Interaction with unregulated actin

In this and the following two sections, we develop and validate a theory for the interaction of finite ensembles of myosin and cMyBP-C with regulated thin filaments (i.e. actin with troponin/tropomyosin). In this first section, Theory I, we consider the interaction of cMyBP-C and myosin with unregulated actin (i.e. actin lacking troponin/tropomyosin). Under these conditions, each molecule acts independently of its neighbors, although global coupling can occur through interaction with a common actin filament [1]. In the second section, Theory II, we consider the interaction of cMyBP-C and myosin with regulated thin filaments. This interaction is considerably more complex than with unregulated actin, because tropomyosin introduces local coupling between molecules [2]. In the third section, Theory III, we consider finite ensemble size.

The remainder of this section presents development and validation of a theory for the interaction of cMyBP-C and myosin with unregulated actin. The principal results are that 1) we can accurately and efficiently describe myosin's interaction with actin in the presence or absence of cMyBP-C; and 2) this interaction is defined by three non-dimensional parameters, f the proportion of myosin molecules that interact with cMyBP-C, b the drag from cMyBP-C and P_C the affinity of cMyBP-C for actin.

1.1 cMyBP-C

In our model, we assume that cMyBP-C interacts with actin via a two-state mechanism (a bound and an unbound state), and that unbinding is, at least approximately, force-independent. The attachment rate constant is k_a^C and the detachment rate constant is k_d^C. Then, at steady-state,

$$v\frac{dn_C}{dx} = k_a^C(1-N_C)(1-N_M)\delta(x) - k_d^C n_C \tag{1}$$

where $n_C(x)$ is the probability density of cMyBP-C being bound to actin; that is, the probability of finding a bound cMyBP-C molecule with extension between x and $x+\Delta x$ is, to first order, $n_C(x)\Delta x$. N_C is the probability of cMyBP-C being bound, $N_C = \int_{-\infty}^{\infty} n_C(x)dx$; N_M is the probability of myosin being bound and $\delta(x)$ is the Dirac delta function.

The assumptions in this equation are

1. that each cMyBP-C molecule competes with, at most, one myosin molecule and can bind only if that myosin is unbound;
2. attachment occurs only with zero extension;
3. each cMyBP-C molecule acts independently of its neighbors.
4. there is a large number of myosin and cMyBP-C molecules.

These latter two assumptions are violated in some of the experiments we consider. We describe how to model such systems in the following two sections (Theory II: Interaction with regulated actin, and Theory III: Approximating small ensembles).

We can solve this equation. First, we integrate across 0

$$n_C(0^-) = -\frac{k_a^C}{v}(1-N_C)(1-N_M) \tag{2}$$

where have used the fact that $n_C(0^+) = 0$ (assuming $v < 0$). Then, integrating from 0 to x, we have

$$n_C(x) = -\frac{k_a^C}{v}(1-N_C)(1-N_M)\exp(-\frac{k_d^C}{v}x) \tag{3}$$

Finally, integrating from $-\infty$ to 0, we have

$$N_C = \frac{k_a^C}{k_d^C}(1-N_C)(1-N_M) \tag{4}$$

So that the probability of cMyBP-C being bound to actin is

$$N_C = \frac{P_C(1-N_M)}{1-N_M P_C} \tag{5}$$

where $P_C = k_a^C/(k_d^C + k_a^C)$. Note that, if cMyBP-C and myosin do not compete for binding sites (i.e., when $N_M = 0$), then $N_C = P_C$.

1.2 Myosin that does not compete with cMyBP-C

Generally, when an ensemble of myosin interacts with actin in the presence of cMyBP-C, there will be two sub-populations of myosin. Myosin molecules in the first sub-population are far enough away from cMyBP-C that they do not compete for actin binding sites. For this sub-population, the attachment rate is k_a^0. Myosin molecules in the second sub-population compete with cMyBP-C, and can only bind if cMyBP-C is unbound. For this sub-population, the attachment rate is $k_a^0(1-N_C)$. We start our derivation considering the first sub-population.

In steady-state, the four-state kinetic scheme for myosin's interaction with actin, shown in Fig. 1C of the main text, is described by the following equations:

$$\begin{aligned} v\frac{dn_1}{dx} &= k_a^0\delta(x-d)N_4 - k_D(x)n_1 \\ v\frac{dn_2}{dx} &= k_D(x)n_1 - k_T[T]n_2 \\ 0 &= k_T[T]\int_{-\infty}^{\infty} n_2 dx + k_h^- N_4 - k_h^+ N_3 \\ 0 &= k_h^+ N_3 - (k_a^0 + k_h^-)N_4 \end{aligned} \tag{6}$$

where $[T]$ is the concentration of ATP, $n_i(x,t)$ is the probability density of being in the i^{th} state, and N_j is the probability of being in the j^{th} state. For simplicity, and to increase computational speed, we assume that attachment occurs only with zero extension (delta function attachment). Note that force-dependent ADP release, written as $k_D(F) = k_D^0 \exp(-\lambda F/k_BT)$ in the main text, can be re-written in terms of molecular extension x using the assumption that myosin is linear elastic with stiffness κ_M

$$k_D(x) = k_D^0 \exp\left(-\frac{\lambda\kappa_M x}{k_BT}\right) \tag{7}$$

In Eqs. 6 and 7, we adopt the notation convention that a rate constant in the absence of some external influence is given the superscript 0. So, for example, ADP release rate in the absence of external force is k_D^0 and attachment rate in the absence of regulatory proteins is k_a^0.

In addition to these differential equations, we have the constraint of conservation of probability

$$1 = \int_{-\infty}^{\infty} n_1 dx + \int_{-\infty}^{\infty} n_2 dx + N_3 + N_4 \tag{8}$$

We can combine the last two equations and this constraint to solve for N_4:

$$N_4 = (1-N_1)\frac{k_T[T]k_h^+}{k_h^+k_a^0 + k_T[T](k_a^0 + k_h^- + k_h^+)} \tag{9}$$

where we use the notation $N_i = \int_{-\infty}^{\infty} n_i dx$. Then, we have one equation to solve:

$$v\frac{dn_1}{dx} = (1-N_1)\frac{k_T[T]k_h^+k_a^0}{k_h^+k_a^0 + k_T[T](k_a^0 + k_h^- + k_h^+)}\delta(x-d) - k_D(x)n_1 \tag{10}$$

Which can be non-dimensionalized

$$\frac{d\hat{n}_1}{dX} = \frac{1}{V}\left[K(1-N_1)\delta(X-1) - \hat{n}_1 e^{EX}\right] \tag{11}$$

where $\hat{k} = (k_T[T]k_h^+k_a^0)/(k_h^+k_a^0+k_T[T](k_a^0+k_h^-+k_h^+))$, $\hat{n}_i = d\cdot n_i$, $K = \hat{k}/k_D^0$, $X = x/d$, $V = v/dk_D^0$, $N_i = \int_{-\infty}^{1}\hat{n}_i dX$ and $E = -\kappa_M\lambda d/k_BT$.

Equation 11 can be solved by first integrating across $X = 1$ (where the delta function dominates) and then integrating from 1 to X (where the delta function is negligible):

$$\hat{n}_1(X) = \left(\frac{-KE}{VE\exp\left(-\frac{e^E}{VE}\right) + KE_1\left(\frac{e^E}{EV}\right)}\right)\exp\left(-\frac{\exp(EX)}{VE}\right) \tag{12}$$

where $E_1(x)$ is the exponential integral function.

Then, using an integrating factor to solve the following non-dimensionalized form of the equation for n_2

$$\frac{d\hat{n}_2}{dX} = \frac{e^{EX}}{V}\hat{n}_1 - \frac{K_T}{V}\hat{n}_2 \tag{13}$$

where $K_T = k_T[T]/k_D^0$, we get

$$\hat{n}_2 = \frac{-KE\exp\left(-\frac{K_T}{V}X\right)}{V^2E\exp\left(-\frac{e^E}{VE}\right) + VKE_1\left(\frac{e^E}{VE}\right)}\int_1^X \exp\left(\frac{K_T}{V}\xi + E\xi - \frac{\exp(E\xi)}{VE}\right)d\xi \tag{14}$$

Force (non-dimensionalized as $\mathcal{F} = F/\kappa_M d$) can be determined from Eqs. 12 and 14 using the equation

$$\mathcal{F} = \int_{-\infty}^{1}(X\hat{n}_1 + X\hat{n}_2)\,dX \tag{15}$$

Motility speed can be determined by solving Eqs. 12 and 14 for V given the constraint that $\mathcal{F} = 0$ in Eq. 15.

1.2.1 Validation I

Eqs. 12, 14 and 15 allow rapid simulation of large myosin ensembles interacting with a single actin filament. Unlike our previous work [1], this derivation is valid at arbitrary ATP, and not just the high ATP limit. It does, however, depend on the assumption that attachment occurs only with zero extension. We examined the effect of this assumption by comparing the predictions of the theory to Monte-Carlo simulations that do not include this assumption (see Section 6 for details). As shown in Fig. 1, the theory accurately (within $\sim 10\%$) replicates experimentally-relevant quantities (e.g. motility velocity as a function of $[T]$, Fig. 1a) as well as binding distributions ($\hat{n}_i$, Fig. 1b).

1.3 Myosin that does interact with cMyBP-C

When myosin interacts with cMyBP-C, we adjust the binding rate to

$$k_a^0(1-N_C) = k_a^0\left(\frac{1-P_C}{1-N_MP_C}\right) \tag{16}$$

then, we have a new expression for the parameter K. In order to differentiate this new parameter from the previous one, we call it K^*. This parameter depends on myosin's binding probability,

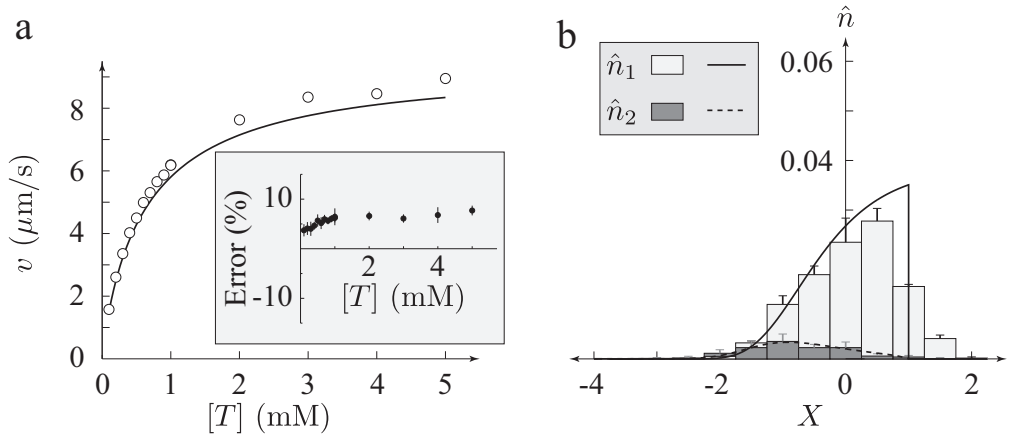

Figure 1: The theory for myosin's interaction with unregulated actin accurately reproduces the behavior of simulated ensembles. a. The theory (solid line) reproduces the speed (v) of simulated actin filaments propelled by myosin ensembles containing $M = 500$ molecules (hollow dots) as a function of ATP concentration $[T]$. A small error (inset) arises because the theory assumes myosin attaches only with zero extension (delta function attachment). b. The theory reproduces simulated distributions of the strongly bound ($\hat{n}_1$) and rigor ($\hat{n}_2$) states at an ATP concentration of $[T] = 2$mM. To minimize the noise in the simulated distributions, we simulated a large ensemble of myosin ($M = 5000$) five times. Mean plus standard deviation is shown.

$N_M^* = N_1^* + N_2^*$ (where, again, we use the superscript * to differentiate variables in the presence of cMyBP-C competition)

$$K^*(N_M^*) = \frac{k_T[T]k_h^+k_a^0(1-P_C)}{k_h^+k_a^0(1-P_C) + k_T[T]k_a^0(1-P_C) + k_T[T](k_h^- + k_h^+)(1-N_M^*P_C)}\left(\frac{1}{k_D^0}\right) \tag{17}$$

So that

$$\hat{n}_1^* = -\frac{(1-N_1^*)K^*(N_M^*)\exp\left(\frac{e^E}{VE}\right)}{V}\exp\left(\frac{-e^{EX}}{EV}\right) \tag{18}$$

and then

$$N_1^* = -\frac{(1-N_1^*)K^*(N_M^*)\exp\left(\frac{e^E}{VE}\right)}{V}\int_{-\infty}^{1}\exp\left(\frac{-e^{EX}}{VE}\right)dX = \frac{(1-N_1^*)K^*(N_M^*)\exp\left(\frac{e^E}{VE}\right)}{EV}E_1\left(\frac{e^E}{EV}\right)$$

solving Eq.13, we have

$$\hat{n}_2^* = -\frac{(1-N_1^*)\exp\left(\frac{e^E}{VE}\right)\exp\left(-\frac{K_T}{V}X\right)K^*(N_M^*)}{V^2}\int_1^X \exp\left(\frac{K_T}{V}\xi + E\xi - \frac{\exp(E\xi)}{VE}\right)d\xi \tag{19}$$

so that, since $N_2^* = \int_{-\infty}^{1}\hat{n}_2^*dX$,

$$N_2^* = \frac{(1-N_1^*)K^*(N_M^*)}{K_T} \tag{20}$$

Together, Eqs. 18 and 19, along with a force constraint (see next section), can be solved for $\hat{n}_1^*$ and $\hat{n}_2^*$.

1.4 Force balance

Suppose that a proportion $(1-f)$ of myosin molecules in a particular ensemble is in the first sub-population, leaving f in the second sub-population. Then, the force generated by that ensemble is

$$\mathcal{F} = (1-f)\int_{-\infty}^{1} X(\hat{n}_1 + \hat{n}_2)dX + f\int_{-\infty}^{1} X(\hat{n}_1^* + \hat{n}_2^*)dX + f\frac{\kappa_c}{\kappa}\int_{-\infty}^{0} X n_c(X)dX \tag{21}$$

The terms on the right hand side are, from left to right, the force from myosin molecules that do not interact with cMyBP-C, the force from myosin molecules that do interact with cMyBP-C, and the force from cMyBP-C. This last integral can be solved explicitly, and is

$$f\frac{\kappa_c}{\kappa}\int_{-\infty}^{0} X n_c(X)dX = fbP_C\left(\frac{(1-N_M)}{1-N_M P_C}\right)V \tag{22}$$

where $b = \kappa_C k_D^0/\kappa_M k_d^C$. Here, it can be seen that cMyBP-C generates a force that is proportional to velocity, acting as a viscous drag.

Given the three non-dimensional parameters f, b and P_C, we can solve Eqs. 12, 14, 18 and Eq. 19 for V, subject to the constraint $\mathcal{F} = 0$ in Eq. 21. While the equations might seem complex, they can be solved numerically on a computer in a fraction of a second.

1.4.1 Validation II

This theory allows rapid simulation of large mixed myosin/cMyBP-C ensembles interacting with a single myosin filament. As before, the derivation depends on the assumption that attachment occurs only with zero extension. Additionally, we assume that we can divide the myosin ensemble into two discrete sub-populations – one that interacts with cMyBP-C and one that does not. We examined the effect of these assumptions by comparing the predictions of the theory to Monte-Carlo simulations (see Section 6 for details). As shown in Fig. 2, the theory accurately (within $\sim 10\%$) replicates experimentally-relevant quantities (e.g. velocity as a function of f) as well as binding distributions ($\hat{n}_i^T = (1-f)\hat{n}_i + f\hat{n}_i^*$).

2 Theory II: Interaction with regulated actin

Myosin's interaction with regulated thin filaments (actin with troponin and tropomyosin) is complex. This complexity arises in part because, at low calcium, myosin molecules are locally coupled. In particular, the attachment rate of one molecule depends on whether neighboring myosin molecules are bound. This coupling violates the independent force generator assumption that underlies the derivation of Huxley-type models (Eqs. 1 and 6).

We have developed a theory for locally coupled myosin ensembles that reasonably predicts the speed of regulated thin filaments in the actin motility assay at low ($\sim$pCa 8) calcium [2]. The theory has two parts: 1) a simplified model of local interactions between myosin molecules; and 2) a differential equation description of the behavior of large myosin ensembles. To model cMyBP-C's effect on actin motility, we have slightly modified the theory. Here, we briefly summarize the main ideas of the theory, more details can be found in Walcott 2013 [2]. We then describe how we have adapted it to model cMyBP-C.

The principal results of this section are that 1) we can accurately and efficiently model myosin's interaction with regulated thin filaments at low calcium; and 2) this interaction requires the specification of two parameters, $\mathcal{C}$ and ε, both of which we have previously estimated.

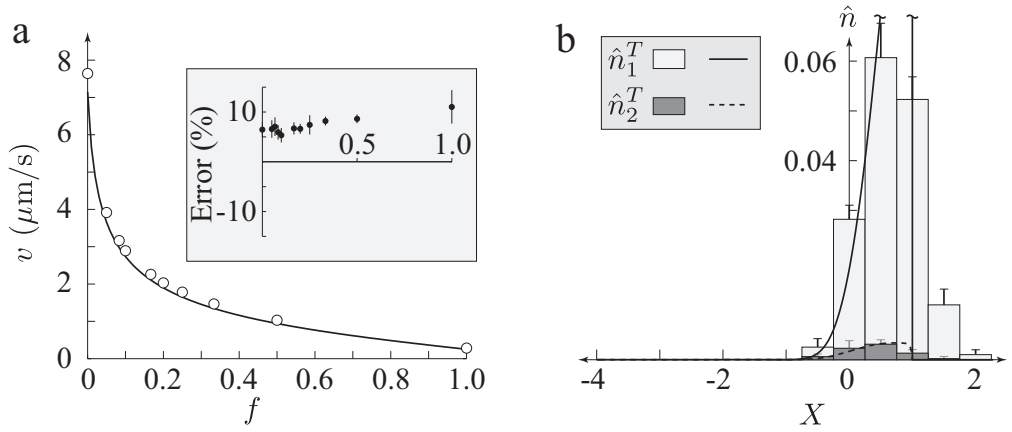

Figure 2: The theory for myosin's interaction with unregulated actin in the presence of cMyBP-C accurately reproduces the behavior of simulated ensembles. a. The theory (solid line) reproduces the speed (v) of simulated actin filaments propelled by myosin ensembles containing $M = 500$ molecules (hollow dots) as a function of f, the proportion of myosin molecules that interact with cMyBP-C. There is a small error (inset). b. The theory reproduces simulated distributions of the strongly bound ($\hat{n}_1^T$) and rigor ($\hat{n}_2^T$) states. Simulations were of 4000 myosin molecules, half of which interacted with cMyBP-C ($f = 0.5$). The mean of five runs is shown, error bars indicate plus one standard deviation. In all simulations and calculations, ATP concentration $[T] = 2$mM, $b = 0.4$ and $P_C = 0.9$.

2.1 Local coupling

Under low calcium conditions, tropomyosin is primarily in the blocked state. Myosin binding is then strongly disfavored. However, in the rare case where a myosin molecule does bind to actin, tropomyosin is locally in the open state, introducing a deformation. This local deformation decreases the energetic cost of the binding of nearby myosin molecules. Even in the simplified case that tropomyosin is modeled as an ideal elastic beam constrained to move on a two-dimensional plane, quantifying this effect is complex. Tropomyosin's shape and the energy of deformation depend both on details of tropomyosin's mechanical properties and the details of its interaction with actin [e.g. 3].

We introduced a simplification of this system that reasonably approximates its behavior and is largely independent of molecular details. Here, we summarize this simplification; more details and validation can be found in Walcott 2013 [2]. The central idea is that when nearby myosin molecules bind, the intervening tropomyosin remains relatively straight (see Fig. 1E of the main text and Fig. 3a). We define tropomyosin's interaction with actin by a potential energy density W that, in general, depends on tropomyosin's azimuthal position on actin x and distance along actin y (Fig. 3a). It is convenient to assume that variations along actin can be averaged out [e.g. 3]. The potential energy density then depends only on azimuthal position, $W(x)$. If the binding of one myosin introduces an azimuthal displacement of length ℓ to tropomyosin, then the overall energy of the tropomyosin between the two bound molecules is $W(\ell) \cdot s$, where s is the distance between the molecules (see Fig. 3a). Since $W(\ell)$ is a constant, the binding energy then increases linearly with the separation between molecules (Fig. 3c).

Since the deformation of tropomyosin is local, we expect that if the two myosin molecules

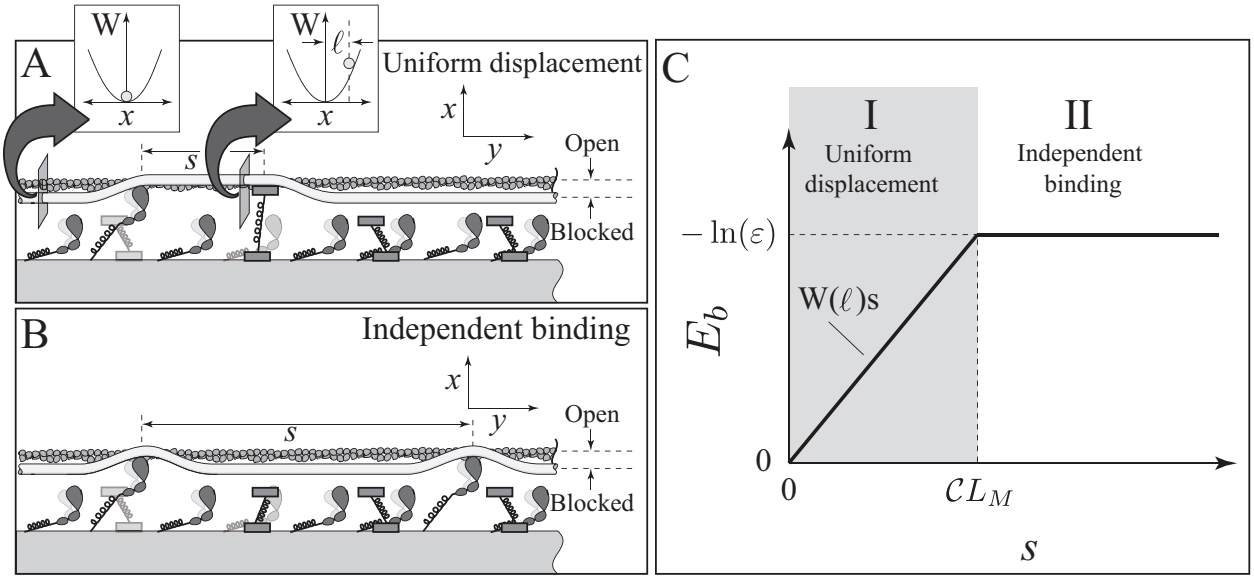

Figure 3: A simple model that defines local coupling. A. When two nearby molecules bind, they introduce a uniform displacement of tropomyosin into the open state. The energy density of that state is $W(\ell)$, with the energy density of the undeformed state $W(0) = 0$ (insets). B. When distant molecules bind, they introduce identical deformations in tropomyosin. They are independent. C. Binding energy (E_b, measured in units of k_BT) as a function of separation between molecules, s. For a uniform displacement, the energy is $W(\ell)s$, while for independent binding it is $-\ln(\varepsilon)$. The transition between the two regimes occurs at $\mathcal{C}L_M$, where L_M is the spacing between molecules.

are separated by a sufficient distance, they act independently (Fig. 3b). Under these conditions, the energy required for the second myosin to bind is the same as for the first molecule, and is independent of the distance separating the myosin (Fig. 3c). Assuming that the transition between the two regimes is abrupt, then the energy for myosin binding (E_b) initially increases linearly with the separation between molecules (s) and then transitions to being independent at a critical separation. This local coupling is then described by two parameters: $\mathcal{C}$, which defines this critical separation distance and ε which defines the energy required for an isolated myosin molecule to bind to regulated actin (Fig. 3c). This simplified model does a reasonably good job of estimating the binding energy for different choices of the potential energy density function $W(x)$ [2].

Given the following assumptions, we can use the binding energy E_b to define local coupling

- Regulation only affects attachment rate (k_a)
- Attachment depends on the binding energy, E_b, as $k_a = \exp(-E_b/k_BT)k_a^0$
- Spacing between myosin molecules, L_M, is roughly constant

Then, considering the binding of a myosin whose nearest bound myosin to the left is i molecules away, and nearest bound myosin to the right is j molecules away

$$k_a(i,j,\mathcal{C},\varepsilon) = \begin{cases} \varepsilon k_a^0 & : \quad i,j \geq \mathcal{C} \\ \varepsilon^{i/\mathcal{C}} k_a^0 & : \quad i < \mathcal{C}, j \geq \mathcal{C} \\ \varepsilon^{j/\mathcal{C}} k_a^0 & : \quad i \geq \mathcal{C}, j < \mathcal{C} \\ \varepsilon^{(i+j-\mathcal{C})/\mathcal{C}} k_a^0 & : \quad i,j < \mathcal{C}, i+j > \mathcal{C} \\ k_a^0 & : \quad i+j \leq \mathcal{C} \end{cases} \tag{23}$$

This equation relates a given myosin's binding rate, k_a, to how it binds in the absence of tropomyosin inhibition, k_a^0, depending on the state of nearby molecules.

2.2 Differential equations

When each myosin molecule in an ensemble acts independently from its neighbors, i.e. when they act as independent force generators, the state of the ensemble is completely specified by the average state of each molecule. That is, equations like Eqs. 1 and 6 can specify ensemble behavior by giving expressions for the time evolution of the average probability of finding a given myosin molecule in a particular biochemical state. The essential problem with modeling locally coupled myosin ensembles is that their behavior depends on how the biochemical states are distributed in the ensemble. For example, two ensembles with the same number of bound molecules (and thus the same average binding probability) would behave differently if those bound molecules are clustered together in one ensemble and spread apart in the other. Thus, equations like Eq. 1 and 6 are an incomplete description, and any successful model of locally coupled ensembles must include an expression for the time-evolution of this clustering.

We developed an approximation that allows the time-evolution of the clustering to be described by a set of linear ODEs [2]. The assumptions of this approximation are

- There are relatively few molecules bound
- The bound molecules are locally clustered
- Binding (at rate k_b) and unbinding (at rate k_u) are independent of force

- Local coupling is defined by Eq. 23

With these assumptions, when an isolated molecule binds, it locally displaces tropomyosin into the open state. If a neighboring molecule subsequently binds, it displaces the intervening tropomyosin into the open state, as long as the two molecules are closer than $\mathcal{C}$ molecules apart (as shown in Fig. 1E of the main text and Fig. 3a). We can keep track of the probability of finding a cluster of i activated molecules – that is, a region of the thin filament that spans i myosin molecules where tropomyosin is entirely in the open state.

The ODEs that describe $c_i(t)$ are, for $i > 1$

$$\frac{dc_i}{dt} = 2k_u \sum_{j=1}^{\mathcal{C}-1} N_b(1-N_b)^{j-1} c_{i+j} - 2k_b \sum_{j=1}^{\mathcal{C}-1} \varepsilon^{j/\mathcal{C}} c_i - 2k_u c_i + 2k_b \sum_{j=1}^{\mathcal{C}-1} \varepsilon^{j/\mathcal{C}} c_{i-j} \tag{24}$$

where N_b the binding probability. The upper bound of the last sum must be adjusted to $i-1$ for $i < \mathcal{C}$. The ODE for $i = 1$ is

$$\begin{aligned} \frac{dc_1}{dt} \quad = \quad & 2k_u \sum_{j=1}^{\mathcal{C}-1} N_b(1-N_b)^{j-1} c_{1+j} - 2k_b \sum_{j=1}^{\mathcal{C}-1} \varepsilon^{j/\mathcal{C}} c_1 - k_u c_1 + \cdots \\ & \varepsilon k_b \left(1 - \sum_{j=1}^{\infty} [i + 2(\mathcal{C}-1)] c_i\right) \end{aligned} \tag{25}$$

In steady-state, these are a set of linear equations and they can be solved by a matrix inversion. Note that the final sum in Eq. 25 goes to infinity. When implementing the theory, we truncated this sum at 300.

2.3 cMyBP-C

We now assume that activation is due entirely to cMyBP-C. At the high ATP concentrations (2mM) of the experiments we model, where myosin's duty ratio is very small, we expect that this assumption is reasonable. At lower ATP concentrations, myosin contributes to thin filament activation and cannot be neglected [e.g. 9]. Under these conditions, this assumption is unreasonable, but we can still perform Monte-Carlo simulations (see section 6).

Given that activation is due entirely to cMyBP-C, in Eqs. 24 and 25, we have $k_u = k_d^C$, $k_b = k_a^C$ and $N_b = P_C$. We further assume that the system has reached steady-state, which allows us to specify the steady-state distribution of c_i from P_C (recall that $P_C = k_a^C/(k_a^C + k_d^C)$).

Then, the probability of cMyBP-C being bound to actin is

$$\eta_C = c_1 + \sum_{i=2}^{\infty} \left(2 + (i-2)P_C\right) c_i \tag{26}$$

and the fraction of the actin filament in the open state is $\phi = \eta_C/P_C$. To translate this to an actin velocity (v_r), we use the equation of Uyeda et al. 1990

$$v_r = v_0 \left(1 - (1 - N_M)^{M\phi}\right) \tag{27}$$

where v_0 is the velocity in the absence of regulation and N_M is the average probability of being bound. These values are determined as described in Part 1. M is the number of myosin molecules in the ensemble.

2.4 Validation

To check model assumptions (e.g. that activation is due entirely to cMyBP-C), we compared the theory to Monte-Carlo simulations. Comparing simulated and predicted actin sliding speed, the agreement is reasonable, particularly when P_C is large (Fig. 4a). For smaller P_C, the theory underestimates the motility speed. This underestimation occurs because as P_C becomes more comparable to myosin's binding probability ($N_M \approx 0.1$), it is unreasonable to assume that myosin contributes negligibly to activation. In support of this explanation, at a given value of P_C, we can get better agreement between theory and simulation by decreasing myosin's binding probability (Fig. 4b).

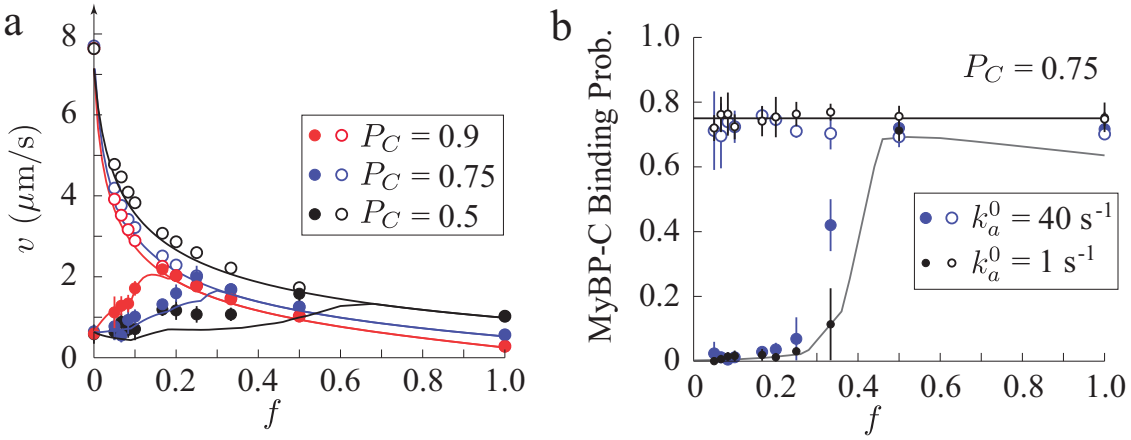

Figure 4: The theory (solid lines) reasonably agrees with simulations of myosin's interaction with regulated thin filaments (filled symbols) and with actin alone (hollow symbols). a. The theory reproduces the speed (v) of simulated thin filaments propelled by myosin ensembles containing $M = 500$ molecules as a function of f, the proportion of myosin molecules that interact with cMyBP-C. While error increases with decreasing cMyBP-C binding affinity (P_C), the theory still captures the qualitative behavior. b. At low cMyBP-C affinity (small P_C) differences between theory and simulation arise because myosin's contribution to activation is not negligible. Agreement between theory (line) and simulation (dots) is improved by lowering myosin's binding probability via a decrease in attatchment rate from $k_a^0 = 40\text{s}^{-1}$ (large symbols) to $k_a^0 = 1\text{s}^{-1}$ (small symbols). Note that the theory's assumption that binding probability is small becomes violated at $f \approx 0.5$, leading to deviations between theory and simulation, but these errors have little effect on predicted velocity.

3 Theory III: Approximating small ensembles

A critical assumption in Part I of the theory is that ensemble size is large. In motility experiments, where less than 100 myosin molecules interact with an actin filament, this assumption leads to a roughly 30% over-estimate of actin filament speed [e.g. 1]. To approximate these smaller ensembles, we introduced a correction.

Comparing theoretical predictions of actin speed to simulations of 50 myosin molecules, we find that error is small for slow speeds ($< 2.5\mu$m/s) and increases roughly in proportion to speed for faster speeds ($> 2.5\mu$m/s, see Fig. 5a). This increase is largely independent of parameters.

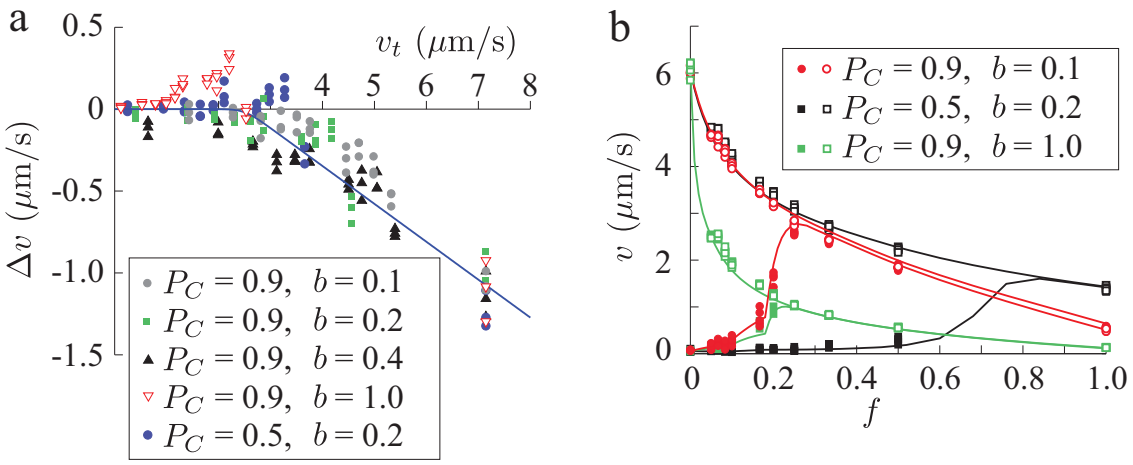

Figure 5: A correction term allows the theory to simulate the behavior of the small myosin ensembles ($M = 50$) appropriate for motility experiments. a. The difference between theoretical speed and simulated speed (Δv) as a function of theoretical speed (v_t) is reasonably described by Eq. 28. The deviation is largely independent of parameters. b. When corrected, the theory describes simulations of actin motility speed in the absence (hollow symbols) and presence (filled symbols) of regulation.

The difference between the theoretical speed (v_t) and the simulated speed (v_s) was fit with the equation (Fig. 5a)

$$\Delta v = v_t - v_s = p_1(v_t - v_0)\frac{e^{p_2(v_t - v_0)}}{1 - e^{p_2(v_t - v_0)}} \tag{28}$$

with $v_0 = 2.5\mu$m/s, $p_1 = 0.23$ and $p_2 = 0.012$. When this correction term is included, the theory reasonably reproduces simulation results for small ensembles and variable b, P_C and f (Fig. 5b).

We have therefore derived a theory that describes the interaction of myosin with thin filaments, with and without regulation, in the presence of variable amounts of cMyBP-C. There are three unknown parameters in the model,

1. f, the proportion of myosin molecules that interact with a cMyBP-C molecule, that determines the importance of competition;
2. b, defined as $b = \kappa_C k_D^0/\kappa_M k_d^C$, that determines the importance of viscous drag;
3. P_C, defined as $P_C = k_a^C/(k_d^C + k_a^C)$, that determines cMyBP-C's affinity for actin.

In contrast to Monte-Carlo simulations, the theory lacks stochastic noise and is efficient. These properties allow us to use optimization-of-fit to estimate parameters.

4 Data fits and sensitivity analysis

In this section, we fit our theory of myosin's interaction with regulated thin filaments in the presence of cMyBP-C to experimental measurements of actin motility [5, 6]. The principal results are that 1) a mechanism that includes activation, drag and competition fits the data, while models lacking either drag or competition cannot; and 2) the best-fit parameters are $a = 0.9 \pm 0.2$ the parameter that governs the importance of competition, $b = 0.13 \pm 0.05$ the parameter that governs

the importance of viscous drag, and $P_C = 0.83 \pm 0.09$ the parameter that governs cMyBP-C's affinity for actin.

4.1 Relating f to cMyBP-C concentration

We fit the model to measurements of regulated thin filament speed at high and low calcium and in the presence of variable amounts of cMyBP-C. To fit these data, we had to relate cMyBP-C concentration to the parameters of the model. The theoretical model of actin motility has three parameters two of which, b (non-dimensional drag of a bound cMyBP-C) and P_C (cMyBP-C affinity for actin), are intrinsic properties of a single cMyBP-C molecule and so are independent of cMyBP-C concentration. The third, f (the probability that a given myosin molecule interacts with cMyBP-C), is a function of cMyBP-C concentration.

As cMyBP-C concentration is increased from zero, the number of molecules capable of interacting with a given actin filament (M_C) should increase linearly. Eventually, however, the actin filament should become completely saturated with cMyBP-C. If actin affinity is strong, then the number of cMyBP-C molecules capable of interacting with an actin filament is

$$\begin{aligned} M_C = \alpha[\text{MyBP-C}] \quad &: \quad [\text{MyBP-C}] < C_{crit} \\ M_C = \alpha C_{crit} \quad &: \quad [\text{MyBP-C}] \geq C_{crit} \end{aligned} \tag{29}$$

where α is a proportionality constant. If these molecules are spaced evenly, then

$$f = a\frac{M_C}{M} \tag{30}$$

where $a = \ell_C / L_M$, the distance on actin that is occluded by cMyBP-C binding (ℓ_C) divided by the spacing between myosin molecules (L_M, see Fig. 1 of the main text). Since the actin filament is fully saturated with cMyBP-C when $f = 1$, we have

$$C_{crit} = \frac{M}{a\alpha} \tag{31}$$

Thus, given the proportionality constant α and the parameter a, we can determine f from cMyBP-C concentration.

4.2 Pre-processing of data

To minimize experimental error, we desired to fit several experimental measurements from different labs. We selected measurements of Razumova et al. 2006 [5] of regulated actin motility at high and low calcium in the presence of the cMyBP-C fragments C1C2 and C0C2 (see Fig. 1 of the main text for a definition of the domains of cMyBP-C). We concurrently fit measurements of Weith at al. 2012 [6] of unregulated actin motility in the presence of the cMyBP-C fragments C0C3, C0C2, C1C2 and C0C1f, the latter of which includes a portion of the M-motif. Measurements performed by the two labs were different, even with the same fragments (Fig. 6a).

Interestingly, in the absence of cMyBP-C, both labs measured the same actin motility speed ($p > 0.05$, one-way ANOVA). Only in the presence of cMyBP-C do the measurements differ (e.g. Weith et al.'s [6] measurements are different from Razumova et al.'s [5] at [cMyBP-C] = 1μM, $p < 0.05$, one-way ANOVA, Bonferroni post hoc comparisons as implemented in Matlab's "multcompare" function). When the data are visualized, it seems plausible that the observed differences would

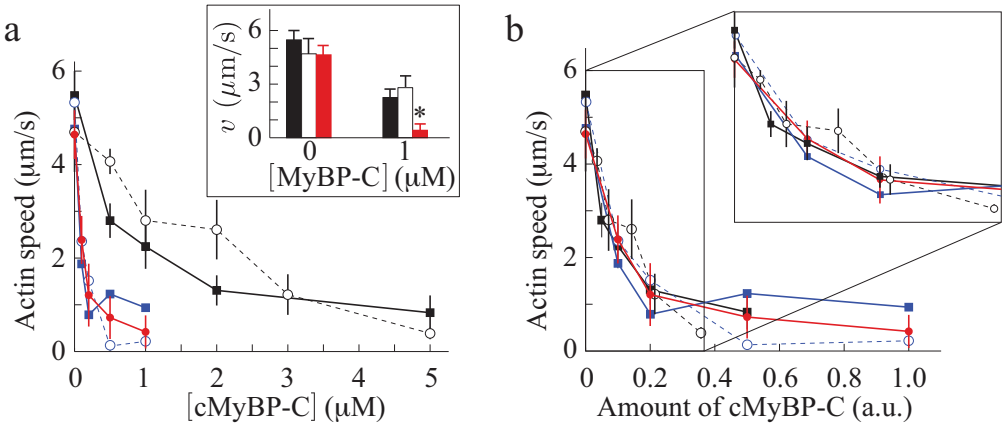

Figure 6: Differences in two labs' measurements of regulated thin filament motility speed as a function of cMyBP-C concentration disappear when the data are rescaled. a. Measurements by Razumova et al. [5] of regulated thin filament motility speed at high calcium in the presence of N-terminal fragments C1C2 (hollow black circles) and C0C2 (black squares) are different from measurements by Weith et al. [6] of motility speed of actin in the presence of C1C2 (hollow blue circles) and C0C2 (blue squares). Shown in red is the average of Weith et al.'s measurements of the fragments C0C3, C0C2, C1C2 and C0C1f. Error bars show standard deviation. Inset shows that the two labs' measurements are not different in the absence of cMyBP-C (one-way ANOVA), but are significantly different ($p < 0.05$, one-way ANOVA, Bonferroni post hoc comparison) in the presence of 1μM cMyBP-C (black bar C0C2 Razumova, hollow bar C1C2 Razumova, red bar, average of different fragments from Weith). b. Rescaling the data of Razumova et al. causes the two labs' measurements to agree. Inset shows a blow-up of low cMyBP-C concentration.

disappear of the concentration of cMyBP-C were re-scaled (Fig. 6a). Indeed, this is the case; differences disappear upon dividing the Razomova et al. [5] concentrations by 10 and 14 for C0C2 and C1C2, respectively (Fig. 6b).

Before fitting the data, we performed one additional modification. Razumova et al. [5] report a minimum resolution of 0.2 μm/s and discarded measurements slower than this value. Thus, measurements near this cut-off will underreport standard deviation. For example, if there were 1000 filaments moving at $v = 0.100 \pm 0.400$, by discarding all measurements less than 0.2, the measured speed could be $v = 0.476 \pm 0.229$. To offset this effect, we increased the standard deviation of their slowest measurements to 0.4 μm/s (these measurements were $v = 0.388 \pm 0.124$, 0.262 ± 0.133, 0.223 ± 0.055, 0.287 ± 0.138). We fit this rescaled data. Importantly, however, our results are independent of this rescaling, since we get similar results by fitting only the measurements of Razumova et al. [5] in the presence of C1C2 (Fig. 7).

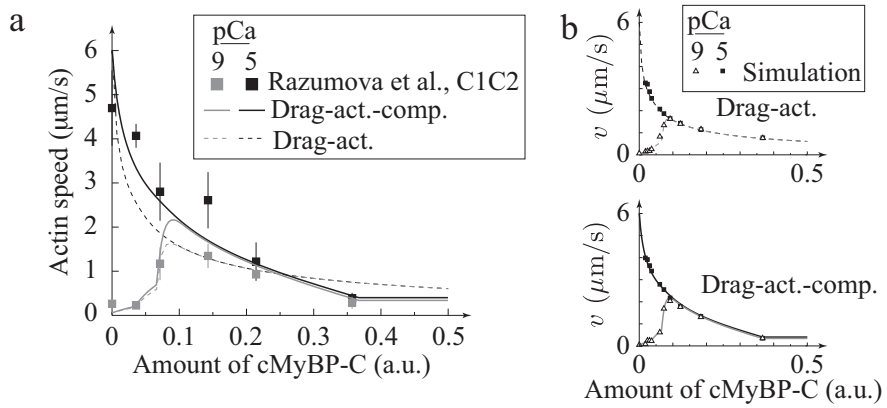

Figure 7: The drag-activation-competition model is consistent with regulated thin filament speed in the presence of variable C1C2 fragments of cMyBP-C, while the drag-activation model is not. a. Best-fits of the theory to the data. The drag-activation-competition fit is not significantly different from the data ($p > 0.05$, χ^2 test) while the drag-activation model is ($p < 0.05$, χ^2 test). b. Comparing theory and simulation of the drag-activation (top) and drag-activation-competition (bottom) best-fits. The good agreement between theory and simulation indicates that our results do not depend on the assumptions of the theory.

4.2.1 Fits without pre-processing

As discussed in more detail in Section 4.2, the data of Weith et al. [6] and the rescaled data of Razumova et al. [5] can be fit with a drag-activation-competition model, but not a drag-activation or a activation-competition model. To show that these results are independent of our pre-processing (rescaling and adjustment of standard deviations) of the Razumova et al. [5] data, we fit their measurements of actin motility in the presence of the C1C2 fragment of cMyBP-C without performing any modifications (Fig. 7a). The drag-activation-competition model is not significantly different from the data ($p > 0.05$, χ^2 test), while the drag-activation model is ($p < 0.001$, χ^2 test). We did not test the activation-competition model because, as discussed in Section 4.2, it is clearly inconsistent with measurements. For each fit, to ensure that the theory faithfully represents the model, we performed Monte-Carlo simulations of the best-fits and compared these results to the theory. The agreement is good (Fig. 7b).

4.3 Fitting data and statistics

Given the parameters a, b and P_C, the theory predicts a relationship between actin velocity, v, and the number of cMyBP-C molecules capable of interacting with the filament M_C. To compare this relationship to experimental measurements, which are reported as a function of scaled cMyBP-C concentration, we scaled it by a parameter α that minimized the χ^2 error for that particular parameter set (a, b, P_C).

We used a Nelder-Mead simplex algorithm (Matlab's "fminsearch" function) to find the parameter set (a, b, P_C) that minimized the χ^2 error between theory and measurement. To maximize convergence speed, we picked values of a (0.6, 0.7, 0.8 and 0.9) and optimized the values of b and P_C. To ensure global convergence, we started optimizations from random initial seeds and visualized the landscape. Optimal parameter values were $a = 0.9$, $b = 0.13$ and $P_C = 0.83$. The best-fit χ^2 value was 34.6, while the critical χ^2 value (at which $p = 0.05$) was 38.89, indicating that the theory was not significantly different from the data (Fig. 8a). To ensure that the theory faithfully represents the model, we performed Monte-Carlo simulations of the best-fit with $a = 1$ and compared the result to the theory. The agreement is good (Fig. 8b). Thus, we conclude that the drag-activation-competition model is not significantly different from the data.

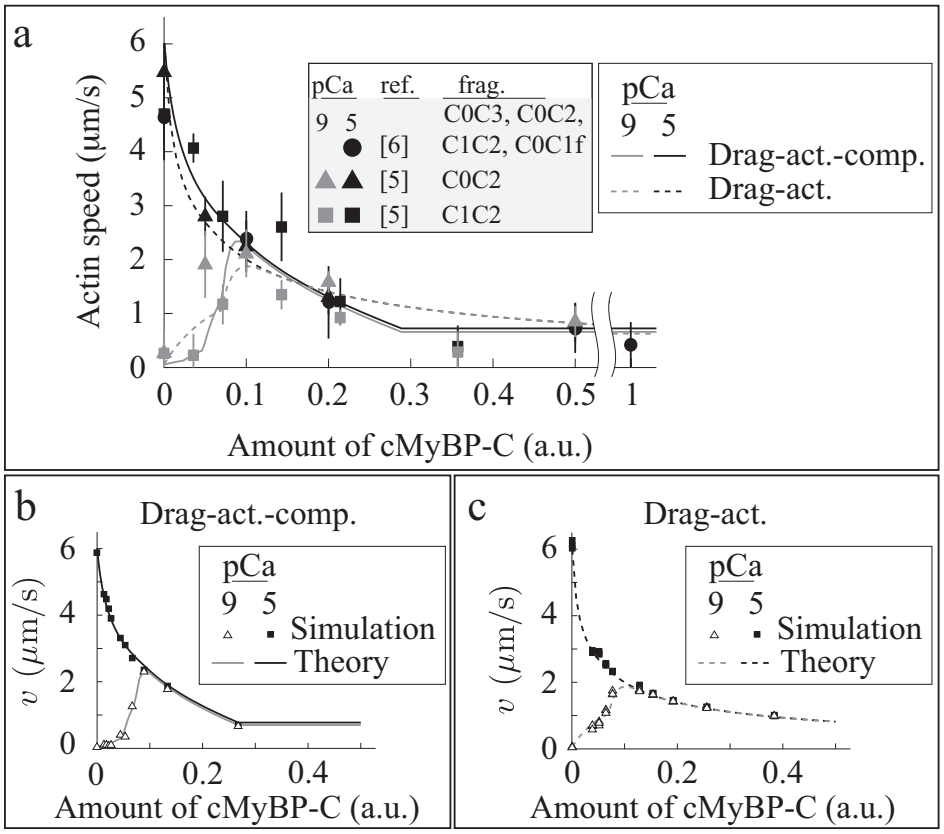

Figure 8: Theory and simulation are consistent. a. A variation on Fig. 2 of the main text, showing the best-fit of the drag-activation-competition model and the drag-activation model with the rescaled data. b. Good agreement between theory and simulation of the drag-activation-competition model with best-fit parameters at $a = 1$. The agreement is reasonable. c. Good agreement between theory and simulation of the drag-activation model with best fit parameters.

For the drag-activation model, we eliminated competition by setting $a = 0$. Again, we used a Nelder-Mead simplex algorithm (Matlab's "fminsearch" function) to find the set of parameters b and P_C that minimized the χ^2 error between theory and measurement. To ensure global convergence, we started optimizations from random initial seeds. Optimal parameter values were $b = 0.61$ and $P_C = 0.99$. The best-fit χ^2 value was 51.8, while the critical χ^2 value (at which $p = 0.05$) was 38.89, indicating that the theory was significantly different from the data ($p < 0.005$, Fig. 8a). To ensure that the theory faithfully represents the model, we performed Monte-Carlo simulations of the best-fit and compared the results to the theory. The agreement is good (Fig. 8c). Thus, we conclude that the drag-activation model, being significantly different from the data, can be rejected.

For the activation-competition model, we eliminated drag by setting $b = 0$. The theory fails for this model, since the cMyBP-C induced decrease in actin speed in the absence of regulation (i.e. either at high calcium or in the absence of regulatory proteins) is caused by a decrease in the number of available myosin motors. This violates a critical assumption in the theory – that there are a large number of motors interacting with actin. Thus, to evaluate whether the model could fit the data, we performed a series of Monte-Carlo simulations. We examined five values of P_C (0.875, 0.9, 0.925, 0.95, 0.975) and three values of a (0.5, 0.75, 1.0). The range of P_C was picked after doing a series of exploratory simulations; one would expect P_C to be near 1 in order to effectively outcompete myosin. We performed 10 simulations at each parameter pair, and compared the average of the 10 to the data. The best fit, at $a = 1.0$, $P_C = 0.925$ had a χ^2 value of 145.8, while the critical χ^2 value (at which $p = 0.05$) was 38.89, indicating that the theory was significantly different from the data ($p < 0.001$). Thus, we conclude that the activation-competition model, being significantly different from the data, can be rejected.

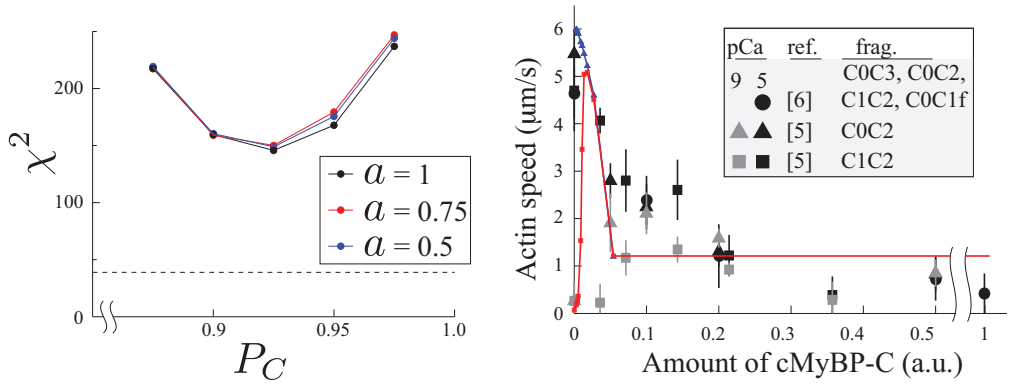

Figure 9: The activation-competition model cannot fit the data. a. A plot of χ^2 values for different values of a and P_C. The best-fit χ^2 value is much greater than the critical χ^2 value (dashed line) that indicates $p = 0.05$. b. The best-fit of the activation-competition model to the data is poor.

The drag-activation-competition model has one more free parameter than the other two models. We therefore performed an F-test to determine whether the drag-activation-competition model fit the data significantly better than the other models. The critical F value for 1, 24 degrees of freedom is 4.26. The drag-activation-competition model is a better fit to the data than both the drag-activation model (F value 11.93, giving $p < 0.005$) and the activation-competition model (F value 77.13, giving $p < 0.001$). Again, we conclude that we may reject the drag-activation and activation-competition models in favor of the drag-activation-competition model.

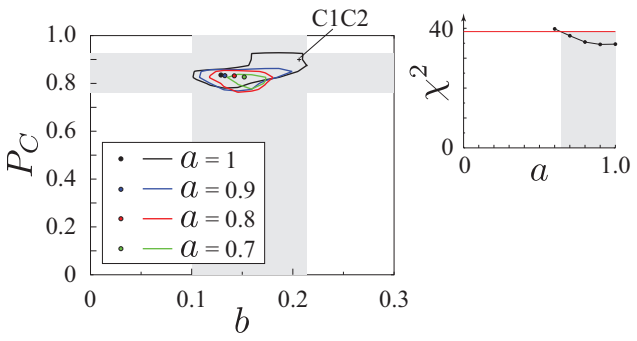

Figure 10: A sensitivity analysis allows estimation of uncertainty in the best-fit parameters. Each closed curve shows the set of parameters (P_C,b) that result in a fit that does not differ from the data ($p > 0.05$, χ^2 test) at a given value of a. These define a range in P_C and b (shaded gray). Inset shows the best-fit χ^2 value at different values of a. The critical χ^2 value is shown as a red line. These define a range in the parameter a (shaded gray).

4.4 Sensitivity analysis

We performed a sensitivity analysis to estimate the uncertainty in our parameter estimates. To do so, we first performed a series of optimizations to find the range of a that resulted in a good fit to the data (i.e. fits that achieved a χ^2 value below the critical value of 38.89). We then evaluated the χ^2 value for the theory for all combinations of the parameters of $a = 0.7, 0.8, 0.9, 1.0$ (selected to span the range of a from the first set of fits), $P_C = 0.700$ – 0.950 at increments of 0.025, and $b = 0.0500$ – 0.2273 at increments of 0.0136 (a total of 616 individual function evaluations). We then used these χ^2 values to identify the set of parameters that could fit the data (Fig. 10). The boundaries of this region are $b = 0.10$ – 0.21, $P_C = 0.76$ – 0.93 and $a = 0.7$ – 1.0. Halving this range gives our uncertainty estimates for the best-fit parameters: $a = 0.9 \pm 0.2$, $b = 0.13 \pm 0.05$ and $P_C = 0.83 \pm 0.09$. Note that the best-fit parameters from only the C1C2 data [5] lie within this region (see section 4.1.1 Fig. 7 and Fig. 10), indicating that pre-processing of the data does not have a large effect on the parameter estimates.

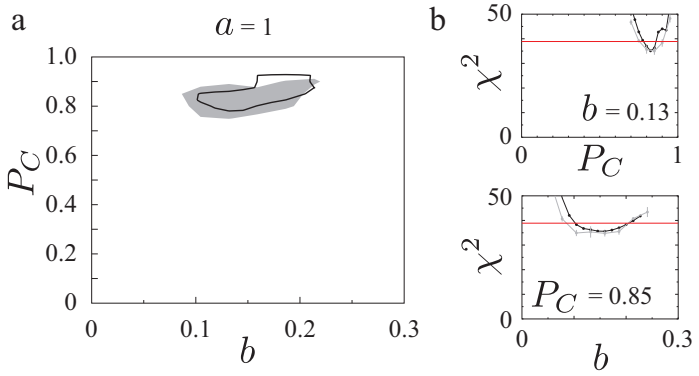

Figure 11: The sensitivity analysis is not dependent on the assumptions of the theory. a. The region of parameter space identified by the theory as being consistent with the data (black outline) is similar to that identified by simulation (gray). b. The χ^2 values calculated from theory (black) and simulation (gray, mean of five simulations, error bars standard deviation) agree.

To ensure that our error estimates were accurate, we performed Monte-Carlo simulations with $a = 1$ over a similar range as our theoretical calculations but with a coarser grid ($P_C = 0.7$ – 0.95 at increments of 0.5, $b = 0.05$ – 0.24 at increments of 0.0273), for a total of 48 simulations. The region of parameter space identified by the Monte-Carlo simulations compares well to our theoretical calculations (see Fig. 11a), as do the calculated χ^2 values (Fig. 11b). This validation gives us confidence in our sensitivity analysis.

4.5 Effects of other parameters

The models presented here build off our previous work [1, 2]. Thus, we only specified the parameters related to cMyBP-C's interaction with actin. However, the parameters in our previous work are estimates, and it is possible that our results would change with different estimates. In particular, for example, the theory overestimates actin speed in the absence of regulation; one might wonder whether, if this error were corrected, the drag-activation model could fit the data.

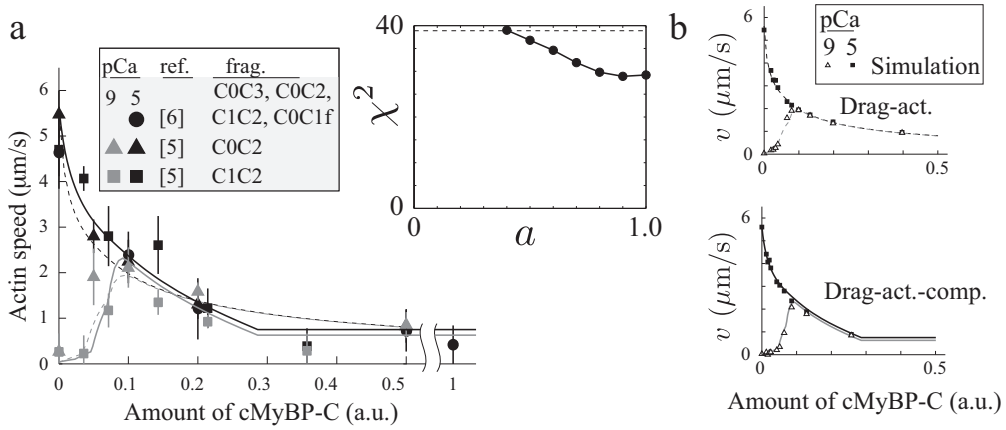

Figure 12: Decreasing ensemble size from $M = 50$ to $M = 40$ myosin molecules improves agreement between model and experiment, but does not change the results. a. Best-fits of the drag-activation-competition model (solid lines, not significantly different $p > 0.05$, χ^2 test) and drag-activation model (dashed lines, significantly different $p < 0.05$, χ^2 test) to data. Inset shows the range of the parameter a in the drag-activation-competition model that is consistent with the data. b. Comparing theory and simulation of the drag-activation (top) and drag-activation-competition (bottom) best-fits. The good agreement between theory and simulation indicates that these results do not depend on the assumptions of the theory, as was the case when $M = 50$.

To investigate this effect, we decreased myosin ensemble size from $M = 50$ to $M = 40$. With this new parameter, the theory more accurately predicted observed actin speed in the absence of regulation. As a result, fits were generally better, with the best-fit χ^2 value being 28.9 (compared to 34.6 with $M = 50$, see Fig. 12). However, the qualitative results remain the same: the drag-activation model remains significantly different from the data ($\chi^2 = 45.9$) and best-fit parameters are similar ($a = 0.9$, $b = 0.12$ and $P_C = 0.84$ compared to $a = 0.9$, $b = 0.13$ and $P_C = 0.83$ with $M = 50$). We therefore believe it unlikely that our results are highly sensitive to our previous parameter estimates.

5 Fits to solution data

The interaction of MyBP-C with actin has been investigated with solution experiments [7]. Fits to these data provide independent estimates of both a and P_C. They do not provide an estimate of b since it depends on the stiffness of MyBP-C, a property that is difficult to infer from solution experiments. The principal result of this section is that parameters estimated from fits to these solution data ($a = 0.8 \pm 0.1$,$P_C = 0.9 \pm 0.1$) are consistent with our estimates from actin motility experiments ($a = 0.9 \pm 0.2$, $P_C = 0.83 \pm 0.09$). Note that although these data are from skeletal muscle MyBP-C [7], the consistency of the best-fit parameters indicates that the action of MyBP-C is likely not isoform-specific.

5.1 Experiments

We considered three separate experiments performed by Moos et al. 1978 [7]. The first experiment demonstrates that myosin S1 (the isolated head domain) binds to the same sites on actin as MyBP-C. In this experiment, actin and S1 were combined in the absence of ATP. Under these conditions, S1 binding is practically irreversible. As one would expect, as more S1 is added, the amount of S1 bound to actin increases until the actin filament is saturated. If MyBP-C is subsequently added, the amount bound to actin decreases as the amount of bound S1 increases. Importantly, the actin filament becomes unable to bind MyBP-C before the actin filament is saturated with S1. Moos et al. recognized that, if S1 binds randomly and irreversibly to actin, this result can be readily explained if MyBP-C binds to several adjacent actin binding sites. We therefore expect that this experiment will be important in defining the parameter a.

The second and third experiments demonstrate that MyBP-C binding to actin inhibits the actin-activated ATPase activity of myosin S1. In particular, in experiment 2, S1 ATPase was measured as a function of MyBP-C concentration at two different actin concentrations. In experiment 3, S1 ATPase was measured as a function of actin concentration for two different concentrations of MyBP-C. As we know the affinity of myosin for actin from our previous work [1], we expect that these experiments will be important in defining the affinity of MyBP-C for actin, P_C. Thus, we expect that simultaneous fits to all of these experiments will provide accurate and precise estimates of both a and P_C.

5.2 Model

For experiment 1, the binding of S1 to actin in an ATP-free solution can be modeled simply with the following kinetic scheme

$$A + S_1 \underset{k^-}{\overset{k^+}{\rightleftharpoons}} A * S_1 \overset{k_a^0}{\rightarrow} AS_1 \overset{k_d}{\rightarrow} A + S_1$$

where actin (A) and S1 (S_1) initially form a weakly-bound collision complex ($A * S_1$) before transitioning to the rigor state (AS_1). We assume that the weakly-bound and unbound states are in rapid equilibrium (i.e. $k^- \gg k_a^0$). Then, the concentration of strongly bound S_1 divided by the total amount of actin is

$$\frac{[AS_1]}{[A_0]} = f_S = (1 - P_U)\frac{(1 + S_0 + P_U K_W/[A_0]) - \sqrt{(1 + S_0 + P_U K_W/[A_0])^2 - 4S_0}}{2} \tag{32}$$

where $S_0 = [S_0]/[A_0]$, $K_W = k^-/k^+$ and $P_U = k_d/(k_a^0 + k_d)$.

It seems reasonable to assume that the distribution of S1 on actin is random and that binding is approximately irreversible (i.e. $k_d << k_a^0$). Then, supposing that MyBP-C comes out of solution to bind to s consecutive actin monomers (A_s) with the following kinetic scheme

$$A_s + C \underset{k_C^-}{\overset{k_C^+}{\rightleftharpoons}} A_s * C \overset{k_a^C}{\rightarrow} A_s C \overset{k_d^C}{\rightarrow} A_s + C$$

then, with the same assumptions as before, we can derive an equation for the concentration of strongly bound MyBP-C divided by the number of available actin binding sites $[A_0^C]$

$$\frac{[AC]}{[A_0^C]} = \hat{f}_C = (1 - P_U^C)\frac{(1 + C_0 + P_U^C K_W^C/[A_0^C]) - \sqrt{(1 + C_0 + P_U^C K_W^C/[A_0^C])^2 - 4C_0}}{2} \tag{33}$$

where $C_0 = [C_0]/[A_0^C]$, $K_W^C = k_C^-/k_C^+$ and $P_U^C = k_d^C/(k_a^C + k_d^C)$.

To find an expression for $[A_0^C]$, we use the assumptions that myosin is distributed randomly on actin and that binding is approximately irreversible:

$$[A_0^C] = [A_0]\left(\frac{1}{s}\right)(1 - f_S)^s$$

Then, the experimentally observed binding probability $f_C = [AC]/[A_0]$, is

$$\frac{[AC]}{[A_0]} = f_C = \left(\frac{1}{s}\right)(1 - f_S)^s(1 - P_U^C)\frac{(1 + C_0 + P_U^C K_W^C/[A_0^C]) - \sqrt{(1 + C_0 + P_U^C K_W^C/[A_0^C])^2 - 4C_0}}{2} \tag{34}$$

For experiments 2 and 3, we want to determine the steady-state ATP consumption of S1 at variable actin and MyBP-C concentrations. Again, we assume that S1 and MyBP-C bind to actin via an initial weakly-bound collision complex that is approximately in equilibrium. Further, we assume MyBP-C unbinds at the same rate as in the absence of ATP (k_d^C), but S1 unbinds at a far faster rate ($k_D^0 = 350\text{s}^{-1}$). Then, the concentration of weakly bound S1 and MyBP-C is

$$\begin{aligned}
[A * S_1] &= \frac{([A]_s + [S] + K_W) - \sqrt{([A]_s + [S] + K_W)^2 - 4[S][A]_s}}{2} \\
[A * C] &= \frac{([A]_s + [C] + K_W^C) - \sqrt{([A]_s + [C] + K_W^C)^2 - 4[C][A]_s}}{2}
\end{aligned} \tag{35}$$

where $[A]_s$ is the concentration of s consecutive actin monomers that have not strongly bound any S1 or MyBP-C, $[S]$ is the concentration of unbound S1 and $[C]$ the concentration of unbound MyBP-C.

Since we have assumed that this equilibrium is reached quickly, we can calculate effective attachment rates, k_p and k_p^C, for S1 and MyBP-C respectively. In particular,

$$\begin{aligned}
k_p &= \frac{[A * S_1]}{[A]_s} k_a^0 \\
k_p^C &= \frac{[A * C]}{[A]_s} k_a^C
\end{aligned} \tag{36}$$

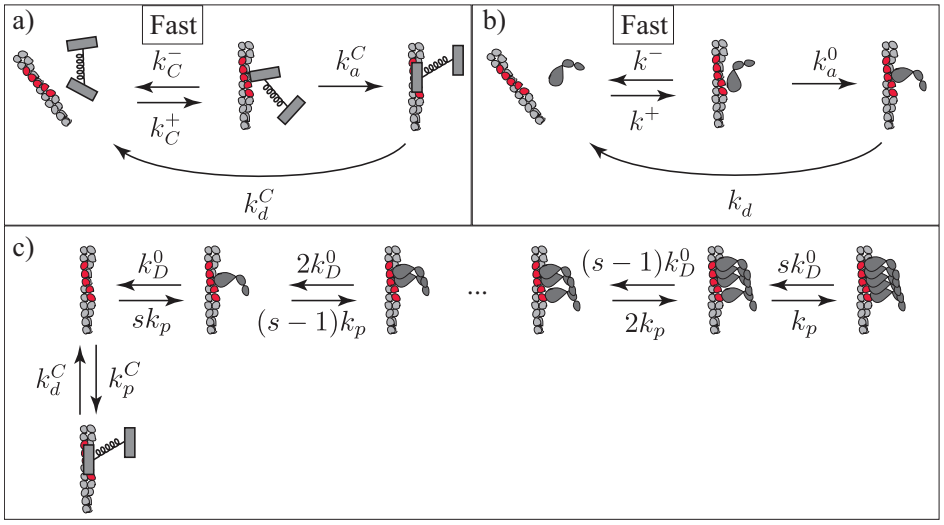

Figure 13: Kinetic schemes for the interaction of MyBP-C and S1 with actin in solution. a. The binding of MyBP-C to actin. An initial collision complex is rapidly formed, followed by a transition to a strongly-bound state. Detachment subsequently occurs. MyBP-C occludes s consecutive actin binding sites (shown in red). b. The binding of S1 myosin to actin in the absence of ATP. An initial weakly-bound state is rapidly formed, followed by a transition to a strongly bound state. In the absence of ATP, detachment occurs at a very slow rate k_d. c. Competition between MyBP-C and S1 myosin for actin binding sites at high (∼mM) ATP. Myosin S1 attaches at a rate k_p and detaches at the rate k_D^0, the ADP release rate in the absence of force. MyBP-C attaches at a rate k_p^C and detaches at k_D^C.

Then, the system obeys a reaction scheme pictured in Fig. 13. The concentration of each possible chemical species obeys a series of ODEs

$$\begin{aligned}
\frac{d[A_s(S_1)_1]}{dt} &= sk_p[A_s] - (k_D^0 + (s-1)k_p)[A_s(S_1)_1] + 2 * k_D^0[A_s(S_1)_2] \\
\frac{d[A_s(S_1)_2]}{dt} &= (s-1)k_p[A_s(S_1)_1] - (2k_D^0 + (s-2)k_p)[A_s(S_1)_2] + 3k_D^0[A_s(S_1)_3] \\
&\vdots \\
\frac{d[A_s(S_1)_s]}{dt} &= k_p[A_s(S_1)_{s-1}] - sk_D^0[A_s(S_1)_2] \\
\frac{d[A_sC]}{dt} &= k_p^C[A]_s - k_d^C[A_sC]
\end{aligned} \tag{37}$$

where $[A_s(S_1)_i]$ is the concentration of s consecutive actin monomers with i strongly bound S1 molecules. To these differential equations, we have three conservation equations

$$\begin{aligned}
S_0 &= [S] + \sum_{i=1}^{S} i[A_s(S_1)_i] \\
C_0 &= [C] + [A_sC] \\
A_0/s &= [A_s] + [A_sC] + \sum_{i=1}^{S} [A_s(S_1)_i]
\end{aligned} \tag{38}$$

where S_0, C_0 and A_0 are the initial concentrations of S1, MyBP-C and actin, respectively. These equations can be solved in steady-state to find the overall ATPase rate per S1, dT/dt

$$\frac{dT}{dt} = \frac{1}{S_0} k_D^0 \sum_{i=1}^{s} i[A_s(S_1)_i]_{ss} \tag{39}$$

where the subscript ss indicates steady-state.

These equations are defined by five parameters, s, K_W, K_W^C, $P_C = 1 - P_U^C$ and $P_U = k_d/(k_a^0 + k_d)$. In addition to these parameters, we were able to fit the data better if we added a small off-set, f_C^0, to Eq. 34.

5.3 Fits and statistics

We optimized fits to the data, maximizing the R^2 of each fit. The fits are reasonably good, with a minimum R^2 of 0.93 (see Fig. 14). Best fit parameters were consistent with those reported in Moos et al. 1978, with $s = 5$ (Moos et al. [7] report 5-6) and $P_C = 0.98$ (Moos et al. [7] estimate the value to be > 0.9). To determine whether these values are consistent with the parameters identified from motility fits, we performed a sensitivity analysis.

5.4 Sensitivity analysis

To perform the sensitivity analysis, we used the best-fits (maximizing R^2) to estimate the standard deviation of the error (assumed constant) of each measurement. Given these standard deviations, we were able to determine the χ^2 value of each fit. We performed a series of optimizations, minimizing this χ^2 value for $s = 4, 5, 6, 7$ and $P_C = 0.74, 0.78, 0.83, 0.87, 0.91, 0.95$ and 0.99. To convert s, the

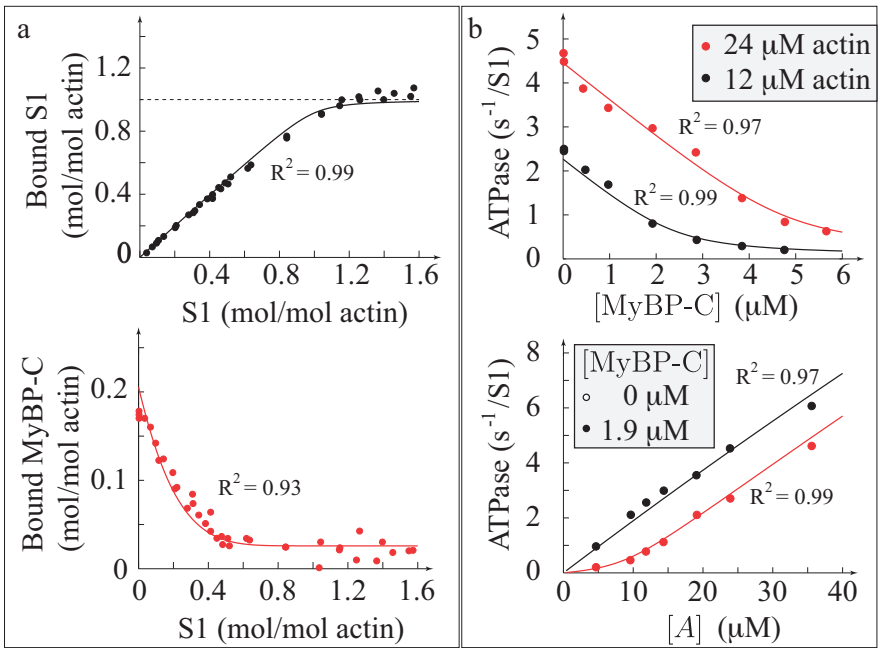

Figure 14: The model, with a single set of parameters, reasonably fits the data of Moos et al. 1978 [7]. a. Experiments performed in the absence of ATP measuring bound S1 myosin (top) and bound MyBP-C (bottom) as increasing amounts of S1 are added. Actin concentration is 16 μM, MyBP-C concentration is 5.4μM. Data are dots, model fits are lines of corresponding color. b. Experiments measuring ATP hydrolysis rate (ATPase) at an ATP concentration of 2mM and S1 concentration of 0.7 μM. Top shows ATPase as a function of MyBP-C concentration at two different actin concentrations. Bottom shows ATPase as a function of actin concentration $[A]$ at two different MyBP-C concentrations. Data are dots, model fits are lines of corresponding color.

number of binding sites occluded by MyBP-C to a, the length occluded by MyBP-C divided by the myosin spacing, we assume that actin subunits are 5.5 nm and that, at high myosin density, myosin spacing is 37 nm [8]. Then, for example, $s = 5$ corresponds to $a = 0.74$.

The sensitivity analysis identifies values of $a = 0.7$–0.9 and $P_C = 0.78$–1.0 that are consistent with the data (i.e. can give fits with a χ^2 value not significantly, $p < 0.05$, different from the data). While the best-fit value of P_C is 0.98, the minimum is quite broad, so we estimate this value as $P_C = 0.9 \pm 0.1$. Our best estimate for $a = 0.8 \pm 0.1$. These parameters overlap the set of parameters that are consistent with our motility fits (see Fig. 15). Thus, it is possible to pick parameter values that could simultaneously fit the motility and solution data, providing further support for the drag-activation-competition model. The parameters that give the best fit to both the actin motility and solution experiments simultaneously are $P_C = 0.83$ and $a = 0.76$.

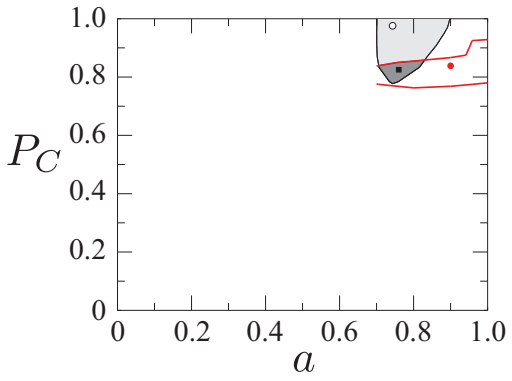

Figure 15: Parameters estimated from fits to solution data are consistent with our estimates from actin motility experiments. The light gray area shows the set of parameters that are consistent with the solution measurements of Moos et al. 1978. The hollow circle shows the best-fit parameters. The red outline shows the set of parameters that are consistent with the actin motility measurement of Razumova et al. 2006 [5] and Weith et al. 2012 [6]. The red dot shows the best-fit parameters. The dark gray region is the set of parameters consistent with both the solution and actin motility measurements. The black square shows the best-fit parameters.

6 Monte-Carlo simulations

In order to derive the differential equations in the Theory sections (Sections 1–3), we made several assumptions. In particular, we assumed

1. myosin and cMyBP-C molecules attach with zero extension;
2. actin velocity can be reasonably approximated by Eq. 27 and a phenomenological correction term (Eq. 28 and Fig. 5);
3. Eqs. 24 and 25 reasonably describe thin filament activation; and
4. at low calcium, thin filament activation is due entirely to cMyBP-C binding.

We do not need to make any of these assumptions to do Monte-Carlo simulations. Thus, throughout this Supplementary Material we test the assumptions of the theory when we compare theoretical calculations to Monte-Carlo Simulations (Figs. 1, 2, 4, 5, 7, 8, 11, and 12). In all cases, the agreement is reasonable, justifying our assumptions. Here, we discuss details of these Monte-Carlo simulations, and make predictions for yet-to-be-conducted experiments at low ATP, where the theory's assumption of negligible myosin activation breaks down.

6.1 General set-up

Simulations modeled the motility of actin due to the interaction of $M = 50$ myosin molecules and varying amounts of cMyBP-C. Simulations were initialized with all cMyBP-C molecules in the unbound state and all myosin molecules in one of the two states unbound to actin. Myosin's distribution between the unbound states was stochastically determined based on the steady state distribution between the two states. Note that, in contrast to the theory that assumes myosin molecules only bind with zero extension, simulated myosin molecules bind with an extension from the sum of two Gaussians, one from the random thermal motion of myosin (with standard deviation $\sigma = \sqrt{k_B T/\kappa_M})$ and another from the random thermal motion of actin (with standard deviation $\sigma = \sqrt{k_B T/(n_c\kappa_C + n_m\kappa_M)}$, where n_c and n_m are the number of bound cMyBP-C and myosin, respectively).

6.2 Gillespie algorithm

The simulations used a modified version of the Gillespie Algorithm. Each molecule is assigned times, selected randomly from an exponential distribution given by the appropriate rate constant, at which the molecule will change to any of the available states. The state transition associated with the shortest of these times, t_s, is assumed to occur. The state of the molecule is then updated and time is increased by t_s. If the state change affects other molecules (e.g. by moving or activating actin), new reaction times are assigned to all affected molecules. However, if the molecule's state change does not affect the other molecules (e.g. myosin switching between unbound states) then a new reaction time is assigned only to the reacting molecule. After each reaction, the position of actin is adjusted to restore mechanical equilibrium. This process is repeated until time reaches a specified value.

6.3 Geometry

For simplicity, we assume that the myosin/cMyBP-C ensemble interacts with an infinitely long, rigid actin filament moving in one dimension. Myosin molecules are spaced evenly and cMyBP-C molecules, when present, are at the same location as a myosin molecule. In simulations with competition, the cMyBP-C molecule competes with the myosin molecule at its location. In simulations with incomplete competition ($a < 1$), cMyBP-C binding precludes concurrent myosin binding with a probability equal to a. We simulated ensembles that contained $f = 0$, 1/20, 1/15, 1/12, 1/10, 1/6, 1/5, 1/4, 1/3, 1/2 and 1 cMyBP-C molecules per myosin molecule. For a ratio of $f = 1/n$, the first cMyBP-C molecule is placed at the ceil$(n/2)$ myosin molecule. After that, cMyBP-C molecules are placed at every n^{th} myosin molecule.

6.4 Average velocity

In the course of each simulation, which typically simulated between 1 and 10 seconds, we recorded the position of the actin filament $x_a(t)$. Once the simulation was complete, we discarded the first 0.2s of $x_a(t)$ to remove non steady-state effects. We then fit $x_a(t)$ to a linear function. The slope of this line was the reported velocity.

6.5 Predictions

The model describes motility experiments in the presence of N-terminal cMyBP-C fragments (section 4). Further, best-fit model parameters are consistent with independent estimates from solution experiments with skeletal MyBP-C and myosin S1 (section 5). With these best-fit parameters, the model also makes predictions of yet-to-be-conducted experiments. Here, we briefly discuss some of these predictions.

The model can be used to estimate various properties of cMyBP-C's interaction with actin. We determined the values of the model's three free non-dimensional parameters, $a = 0.9 \pm 0.2$, $b = 0.13 \pm 0.05$ and $P_C = 0.83 \pm 0.09$, but the model does not explicitly predict, say, the dissociation rate constant of cMyBP-C (k_d^C). Instead, given an association rate for cMyBP-C (k_a^C), we could predict cMyBP-C's dissociation rate from our value of P_C (since $P_C = k_a^C/(k_a^C + k_d^C)$). Alternatively, given a stiffness of cMyBP-C (κ_C), we could predict the dissociation rate from b and our estimates of $k_D^0 = 350\text{s}^{-1}$ and $\kappa_M = 0.3\text{pN/nm}$ (since $b = \kappa_C k_D^0/\kappa_M k_d^C$).

Additionally, with the best-fit parameter values, the model can be used to predict the results of motility experiments performed under different conditions. As a particular example, we simulated measurements of the motility speed of regulated thin filaments (v) in the presence of variable cMyBP-C and ATP ($[T]$) at high (pCa 5) and low (pCa 9) calcium (see Fig. 16). With the model, we can visualize the entire surface, $v([\text{cMyBP-C}], [T])$ (Fig. 16a). These simulations allow us to predict the results of two sets of experiments: 1. rigor activation, the biphasic response of motility speed at low calcium as a function of ATP [e.g. 9], both in the absence and presence of cMyBP-C (Fig. 16b); and 2. motility speed as a function of cMyBP-C at variable ATP, which is biphasic at low calcium and high ATP [5] (Fig. 16c).

A common feature of these simulations is that the biphasic behavior observed at low calcium (pCa 9) disappears under some conditions. In the model, this is because either low ATP or high cMyBP-C lead to thin filament activation. In particular, if ATP concentration is less than $\sim$ 0.025mM or cMyBP-C concentration is above ~ 0.085 arbitrary units, then the filament is active and biphasic behavior is not observed. Further, since the thin filament is predicted to be active under these conditions, calcium has little effect on motility speed. These predictions could be experimentally tested.

References

[1] Walcott, S., D. M. Warshaw and E. P. Debold. 2012. Mechanical coupling between myosin molecules causes differences between ensemble and single-molecule measurements. *Biophys. J.* 103: 501–5510.

[2] Walcott, S. 2013. A differential equation model for tropomyosin-induced myosin cooperativity describes myosin-myosin interactions at low calcium. *Cell. Mol. Bioeng.* 6:13–25.

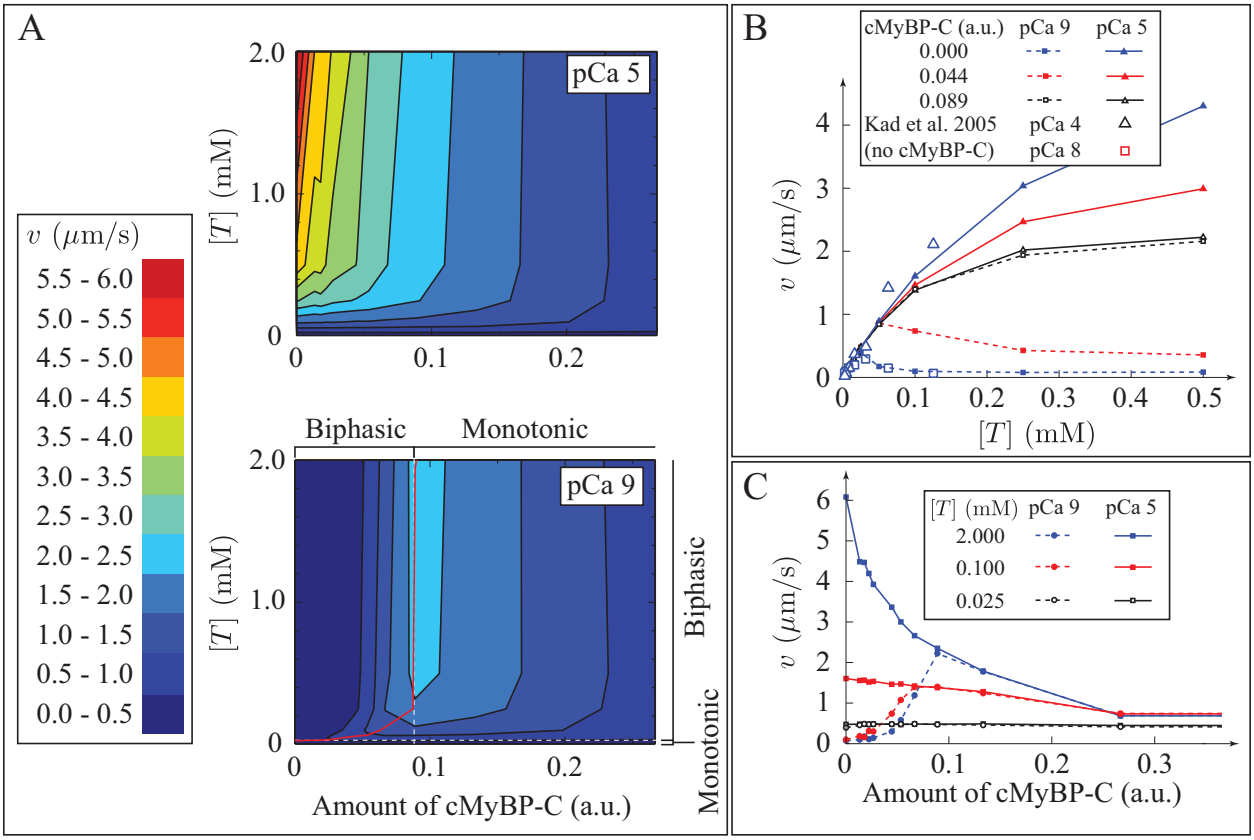

Figure 16: Simulated effects of variable ATP ($[T]$) on the motility speed of regulated thin filaments (v) in the presence of N-terminal fragments of cMyBP-C. a. Contour plots of v as a function of cMyBP-C and $[T]$ at high (top) and low (bottom) calcium. On the low calcium plot, the red line indicates activation of the thin filament. Below or to the right of the line, increasing calcium to pCa 5 affects motility speed by less than 0.125μm/s. The dashed white lines indicate the transition between biphasic and monotonic measurements of $v([T])$ at constant cMyBP-C (vertical) and v(cMyBP-C) at constant $[T]$ (horizontal). b. Predictions of measurements of $v([T])$ at constant cMyBP-C. The cooperativity parameters ($\mathcal{C}$ and ε) were picked to fit data from Kad et al. [9] in the absence of cMyBP-C. Biphasic behavior observed at low calcium leads to a local maximum in v (blue). Addition of cMyBP-C shifts this maximum to the right (red) and eventually leads to monotonicity (black). c. Predictions of measurements of v(cMyBP-C) at constant $[T]$. Biphasic behavior observed at low calcium and $[T] = 2$mM leads to a local maximum in v (blue). Decreasing $[T]$ shifts this maximum to the left (red) and eventually leads to monotonicity (black).

[3] Smith, D. A., R. Maytum and M. A. Geeves. 2003. Cooperative regulation of myosin-actin interactions by a continuous flexible chain I: actin-tropomyosin systems. *Biophys. J.* 84: 3155–3167.

[4] Uyeda, T. Q. P., S. J. Kron and J. A. Spudich. 1990. Myosin step size: estimation from slow sliding movement of actin over low densities of heavy meromyosin. *J. Mol. Biol.* 214: 699–710.

[5] Razumova, M. V., J. F. Shaffer, A-Y. Tu, G. V. Flint, M. Regnier and S. P. Harris. 2006. Effects of the N-terminal domains of myosin binding protein-C in an in vitro motility assay. *J. Biol. Chem.* 281:35846–35854.

[6] Weith, A., S. Sadayappan, J. Gulick, M. J. Previs, P. VanBuren, J. Robbins and D. M. Warshaw. 2012. Unique single molecule binding of cardiac myosin binding protein-C to actin and phosphorylation-dependent inhibition of actomyosin motility requires 17 amino acids of the motif domain. *J. Mol. Cell. Cardiol.* 52:219–227.

[7] Moos, C., C. M. Mason, J. M. Besterman, I-N. M. Feng and J. H. Dubin. 1978. The binding of skeletal muscle C-protein to F-actin, and its relation to the interaction of actin with myosin subfragment-1. *J. Mol. Biol.* 124:571–586.

[8] D. E. Harris and D. M. Warshaw. 1993. Smooth and skeletal muscle myosin both exhibit low duty cycles at zero load in vitro. *J. Biol. Chem.* 268: 14764-14768.

[9] Kad, N. M., S. Kim, D. M. Warshaw, P. VanBuren and J. E. Baker. 2005. Single-myosin crossbridge interactions with actin filaments regulated by troponin-tropomyosin. *Proc. Natl. Acad. Sci.* 102:16990–16995.